Molecular Dynamics Study of Ice-Vapor Interactions via the Quasi-Liquid Layer

Steven Neshyba[†], Erin Nugent[†], Martina Roeselova[‡], Pavel Jungwirth[‡]

[†]University of Puget Sound, Tacoma, Washington, 98416, USA; [‡]Institute of Organic Chemistry and Biochemistry, Academy of Sciences of the Czech Republic and Center for Biomolecules and Complex Molecular Systems, 16610 Prague 6, Czech Republic.

Keywords: ice surface, surface accommodation coefficient, bulk accommodation coefficient, sublimation, deposition

[*]To whom correspondence should be addressed. E-mail: nesh@ups.edu, phone: +1-253-879-3379

ABSTRACT

Molecular dynamics simulations of ice I_h in a slab geometry with a free basal (0001) surface are carried out at 250 K in order to study the structure and dynamics of the ice/vapor interface, focusing on processes associated with sublimation and deposition. Surface melting, which results in the formation of a quasi-liquid layer, causes about 8% of the molecules originally constituting the surface bilayer to leave their crystal lattice positions and form an outer, highly mobile sublayer. Molecules in this sublayer typically form two H-bonds, predominantly in a dangling-O orientation, with preference for a dangling-H orientation also evident. The remaining 92% of the quasi-liquid layer molecules belong to the deeper, more crystalline sublayer, typically forming three H-bonds in an orientational distribution that closely resembles bulk crystalline ice. Transitions between the quasi-liquid layer and the first underlying crystalline bilayer were also observed on the molecular dynamics simulation time scale, albeit with substantially longer characteristic times. Regarding deposition, a very high (>99%) probability of water vapor molecules sticking to the ice surface was found. 70% of incident molecules adsorb to the outer sublayer, while 30% are accommodated directly to the inner sublayer of the quasi-liquid layer, with an orientational relaxation time of ~2 picoseconds and a thermal relaxation time of ~10 picoseconds. Regarding the mechanism of sublimation, we found that prior to sublimation, departing molecules are predominantly located in the outermost sublayer and show a distinct preference for a dangling-O orientation.

I. Introduction

An important component of climate modeling is accurate representation of the radiative effects of cirrus clouds[1-4]. This depends, in turn, on our understanding of how the various sizes, shapes, and surface characteristics of atmospheric ice particles develop[5-11]. Considerable effort, therefore, has been directed at understanding the molecular-scale processes that govern ice particle growth. If we understood better the mechanisms by which vapor deposition and sublimation took place, we would be in a better position to predict the morphology of atmospheric ice crystals, and hence the radiative properties of cirrus clouds.

One approach to this topic is the use of molecular dynamics (MD) simulations. On a practical level, the expansion of computing and algorithmic capabilities in recent years has made it possible to simulate model systems containing thousands of small molecules over hundreds of nanoseconds. Together with improvements in the representation of intermolecular forces, MD models have allowed researchers to investigate a great variety of surface processes, including the mechanics of freezing and the nature of ion solvation during freezing[12,13].

In designing a molecular dynamics approach to the study of ice-vapor interactions, our strategy has been to target equilibrium or near-equilibrium processes, as opposed to nonequilibrium ones, because fewer assumptions about the ice surface are required. For example, simulation of net deposition from vapor, a nonequilibrium process, would

require representation of surface ice nucleation to a degree of specificity that we are only beginning to understand[14]. In contrast, the ability of an ice surface to adsorb individual incident water vapor molecules is a near-equilibrium process that requires assumptions about the nature of the equilibrated ice-vapor interface, but not about nucleation.

The primary aim of this paper is to use molecular dynamics to gain insight into molecular mechanisms underlying near-equilibrium processes relevant to ice deposition and sublimation. We construct a model in which the basal (0001) facet of ice is exposed to vacuum, and examine mechanisms of capture from, and escape to, the gas phase, at a nominal temperature of 250 K. We are interested in finding answers to the following questions: What fraction of molecules striking the surface at this temperature stick? On what time scale do orientational and thermal relaxations occur? What is special about molecules that are about to sublimate from the surface? What is the rate of sublimation? What is the ultimate fate of molecules that strike the surface, given near-equilibrium conditions?

The microscopic nature of MD also allows us to extract quantitative information from the simulations, namely values of the surface accommodation coefficient, the bulk accommodation coefficient, and the equilibrium vapor pressure, directly from their microscopic definitions. The surface accommodation coefficient, designated α_s[15], is defined as the number of water vapor molecules that adsorb onto the ice surface, divided by the total number of water vapor molecules striking the surface. α_s can be thought of as a measure of the stickiness of the surface. Several recent studies have suggested that the

surface of condensed water – whether solid or liquid – is very sticky. Molecular dynamics studies of the water-vapor interface by Vieceli *et al*[16], for example, indicate a value of $\alpha_s \sim 1$ when the incident water vapor is thermal and the condensed phase is liquid water; other workers have reported similar theoretical[17,18] and experimental results[19]. Batista *et al*[20], studying much hotter (0.5-1.5 eV) water vapor molecules impinging on a much colder (20-120 K) ice surface, also report a very sticky surface, with $\alpha_s \sim 1$ for most conditions studied; a low value of 0.9 was observed only for molecules approaching the surface with large grazing angles at kinetic energies of 1.5 eV.

Intermediate between these is ice whose surface is covered by a quasi-liquid layer (QLL), which develops at temperatures above 180 K[21]. Given the above-mentioned results, our expectation is that α_s should be ~1 for thermal vapor molecules impinging on a QLL. To our knowledge, no molecular dynamics evaluation of α_s at the QLL has been undertaken yet, although the machinery for doing so is now available. An intermolecular potential good enough to reproduce the melting temperature of ice to within ~16°*C* has recently been introduced[22]. Moreover, because it is relatively easy to set up initial conditions in which many molecules are directed at a surface (one at a time) and because the relevant time scales for thermal relaxation are likely to be tens of picoseconds (by comparison with liquid water[16]), good statistics for α_s can be anticipated. These statistics, in turn, offer the possibility of gaining insight into the mechanisms of adsorption.

A second parameter important for ice crystal growth that one can evaluate using MD is the equilibrium vapor pressure, P_{vap}, associated with a specific facet. Relatively little MD

work has been done along these lines. Carignano *et al*[14] report that their MD simulations indicate a sublimation rate "consistent with the water vapor pressure under the conditions of the simulations", but do not supply quantitative results or specific mechanisms. Since sublimation events are infrequent on a MD timescale, we can anticipate that long (>100 nanosecond) trajectories are required to obtain even modest statistical confidence.

Thirdly, we look at inter-bilayer dynamics to gauge the rate of exchange between the QLL and underlying ice bilayers. In combination with P_{vap}, this information allows us to calculate a layer-specific bulk accommodation coefficient, α_b, defined as the probability an individual water molecule, once adsorbed, will be taken up by the condensed phase (its other fate being to return to the gas phase).

The paper is structured as follows. In section II we describe the structure of slab model, the intermolecular potential, and simulation parameters. In section III we present our results, including the calculation of α_s, α_b, and P_{vap}, the distribution of orientations of adsorbed molecules, and the statistics of sublimation *vis a vis* a Poisson-derived distribution. In section III we discuss adsorption mechanisms proposed by Batista *et al*[20], Andersson *et al*[23], and others in light of the present results. Section IV summarizes our main conclusions.

II. Methods

Our approach follows a well-established protocol for carrying out molecular dynamics simulations of extended slabs[24-27], in which periodic boundary conditions are imposed in all three dimensions on a rectangular prismatic simulation box. A slab of ice occupies the entire (x-y) length and width of the simulation box, 3.59 nm × 3.11 nm. In the z-dimension, the slab occupies 3.32 nm, but the simulation box is elongated to 7 nm. This elongation creates two ice-vapor basal (0001) interfaces with enough distance between them that negligible potential energy interactions occur through the z-periodic boundary. The slab itself is comprised of ten bilayers of 128 molecules each, oriented such that the prismatic surface of the ice is perpendicular to the x-axis. The initial geometry of the slab was constructed using the proton-disordering algorithm of Buch *et al*[28], and subsequently annealed for a few hundred picoseconds before conducting production runs.

Water molecules are modeled as rigid rotors, interacting with one another via a 6-site intermolecular potential developed by Nada and van der Eerden[22] specifically for ice simulations. Constant NVT simulations were carried out using Gromacs software[29] with a 1-femtosecond integration step, using Berendsen temperature coupling set to 250 K with a time constant of 0.1 picosecond. To calculate long-range Coulomb interactions, particle-mesh Ewald summation[30] was used with a relative tolerance of 10^{-5}, 4^{th} order cubic interpolation, and a Fourier spacing parameter of 0.12. For van der Waals interactions and the real space part of the Coulomb interaction, a cut-off distance of 0.7 nm was used.

In preparation for a study of the surface accommodation of vapor molecules, assemblies of eight gas-phase molecules, with attractive parts of the intermolecular potential disabled, were thermally equilibrated to a temperature of 250 K in a separate simulation, using a simulation box of the same dimension and periodic boundary conditions as used in production runs. Approximately 600 molecules prepared in this way were analyzed to assure a mean and standard deviation of energy to be consistent with a Maxwell distribution. Each accommodation simulation was constructed such that one gas-phase molecule was inserted into the simulation box containing an ice slab. This molecule was placed initially at a height of z=6.5 nm, i.e., 1.5 nm distant from the ice surface, for a 15-picosecond simulation.

III. Results

Figure 1 shows a prismatic-side view of an equilibrated ice slab. The unit cell is displayed in solid colors, with periodic images on the left and right. Both basal surfaces are less ordered than interior layers. A water vapor molecule (also with two periodic images), having recently escaped from the upper surface, appears above the slab; within a few picoseconds it will cross the vertical boundary and strike the lower surface from below.

The vertical density profile of the slab, based on the z-coordinate of oxygen atoms averaged over tens of nanoseconds, is shown in Figure 2. The figure clearly shows bilayer doublets in inner layers of the slab, and slight degradation of the outermost ones.

Figure 2 allows us to unambiguously define sublayers ε_1, ε_2, collectively designated hereinafter as the QLL. Layers μ_1 and $\mu_{i>1}$ are referred to as the near-surface bulk layer and the bulk layers, respectively. The population of the QLL varies slightly on a time scale of tens of nanoseconds because of sublimation (sublimating molecules leaving one surface and arriving at the other surface). The mean population of the ε_1 sublayer is about ten molecules, or ~8% of the QLL.

Table 1 displays layer-by-layer mean vertical binding energies of water molecules based on five nanoseconds of simulation time. Vertical binding energy is defined here as the negative of the sum of potential energies between a given molecule and the rest of the slab. The uncertainties quoted are one standard deviation about the mean. Assuming an optimal hydrogen bond (H-bond) strength of ~23 kJ/mole[31], we can interpret these data as follows: molecules in sublayer ε_1 make ~2 H-bonds, molecules in sublayer ε_2 make ~3 H-bonds, and molecules in inner layers μ_i make ~4 H-bonds.

It is of interest to examine not only the strength but also the longevity of these bonds. Figure 3 shows the layer-by-layer distribution of long-lived (>1 nanosecond) H-bond coordination numbers. The QLL (ε_1 and ε_2) is predominantly comprised of molecules with no long-lived H-bonds. Bulk layers μ_2 and μ_3, by contrast, are predominantly comprised of long-lived 4-coordinated molecules. Intermediate between these is the near-surface bulk layer, μ_1, which has approximately equal numbers of long-lived 4- and 3-coordinated molecules.

In order to explore the statistics of water vapor deposition, approximately 600 gas-phase molecules, prepared as described in the previous section, were allowed to strike the slab surface one at a time. Figure 4 shows z-coordinates of the oxygen atoms of a subset of these molecules. Two non-sticking trajectories were found (only one is shown in the figure); the result is a surface accommodation coefficient of $\alpha_s > 0.99$. Analysis of the vertical coordinates of these molecules at fifteen picoseconds shows that 70% of sticking molecules end up in the ε_1 layer, while the remaining 30% end up in ε_2.

In an effort to understand the energetics of surface accommodation, time evolutions of vertical binding energies of incident molecules were synchronized to the moment of impact, and averaged over the next ten picoseconds. Note that some of the molecules arrived at the surface too late to be included in this analysis. After excluding these late-comers, we were left with 328 molecules adsorbing to ε_1, and 124 molecules adsorbing to ε_2. Figure 5 shows the resulting energetics analysis. It suggests that thermal relaxation occurs primarily to a vertical binding energy corresponding to ε_1 (see Table 1), i.e., ~2 H-bonds. This result is expected for the 70% of molecules actually adsorbing to ε_1, but it is surprising for the 30% of molecules adsorbing to ε_2. That is, molecules recently adsorbed to ε_2 have only ~2 H-bonds, unlike the mean value of ~3 H-bonds for molecules in ε_2.

To explore the mechanism of sublimation, we defined sublimation events to have taken place whenever the z-coordinate of an oxygen atom crossed the vertical periodic boundary. A total of 37 sublimation events were recorded over 173 nanoseconds of simulation time. It is of interest to examine both the depth and the orientation of

sublimating molecules prior to sublimation. Figure 6 shows the z-coordinate of a representative sample (twelve molecules) ten picoseconds prior to departure from the surface. At that time, eight of the departing molecules were in the ε_1 layer. One picosecond prior to departure, all but two had moved to ε_1.

Sublimation events observed in the MD simulation allow us to estimate a value for the corresponding vapor pressure. We begin with the rate of sublimation,

$$R = \frac{Number\ of\ sublimation\ events}{simulation\ time \times surface\ area} \tag{1}$$

and use a modified Hertz-Knudsen formula[32],

$$P_{vap} = \frac{1}{2} R \sqrt{2 k_B T m} \tag{2}$$

where T=250K, k_B is Boltzmann's constant, and m is the mass of a water molecule. The factor of ½ occurs because there are two ice-vapor interfaces in the model. The resulting value is P_{vap}=240 Pa.

To evaluate an uncertainty in the value of P_{vap}, we undertook a comparison of sublimation statistics with a Poisson model. Considering the occurrence of sublimation events to be Poissonian[33], we write the expected number of sublimation events as

$$N_{departures}(\tau_n) = \left(\sum_{k=1}^{k_{tot}} P(k, \lambda_{n+1}) - \sum_{k=1}^{k_{tot}} P(k, \lambda_n) \right) k_{tot} \quad (3)$$

where τ_n is the time interval between sublimation events, and k_{tot} is the total number of sublimation events (37). The Poisson function P is a function of the average number of sublimation events in a given time interval, $\lambda_n = \frac{k_{\max}}{t_{\max}} \tau_n$, and of the number of events of interest, k. The results, displayed in figure 7, suggest a Poissonian distribution. The uncertainty due to finite simulation time is estimated at <20% of the mean simulated value, hence P_{vap}=240±50 Pa.

We have found Euler angles to be a useful tool for describing orientation statistics. We use the 3-1-3 Euler convention, in which an initial rotation about the z-axis (surface normal) by angle Φ is followed by a rotation about the x-axis by angle Θ[34]. (A third Euler angle specifies a final rotation about the surface normal; we will not be concerned with this angle because any orientational preferences in this dimension would be spread out into the six-fold symmetry of the basal surface, and therefore be less pronounced compared to distributions in the first two angles.) In the molecule-fixed frame, water molecules lie in the y-z plane with axis of symmetry (dipole moment vector) coincident with the z-axis, oxygen in the positive z direction. In this representation, cos(Θ) is the projection of the normalized dipole moment vector onto the laboratory-fixed surface normal. The range of Θ is 0 to π. Since water has C_{2V} symmetry, the non-redundant range of Φ is also 0 to π.

Illustrations of the angle definitions are provided figure 8. In figure 8a, an initial rotation along the z-axis to $\Phi=\pi/2$ is followed by rotation along the x-axis to $\Theta=\pi/2$. The range of orientations corresponding to the second step, together with orientations that deviate only slightly from them, can be written $\Phi\approx\pi/2$ and $\Theta\approx 0\text{-}\pi/2$; molecules in this range are hereinafter designated as "dangling-O". Figure 8b shows x-axis rotation to $\Theta=\pi$ without any prior rotation in the z-axis. The coordinate range $\Phi\approx 0$ or π, $\Theta\approx\pi/2$, corresponds to an orientation similar to the "dangling H-bond"[35]; molecules within this range are hereinafter designated as "dangling-H". Figure 8c is a plan-view snapshot of the basal surface with ε_1 molecules highlighted, showing several admolecules in dangling-H and dangling-O orientations.

We should note that the designations "dangling-H" and "dangling-O" are conventionally used only for surface molecules, hence strictly speaking only applicable to ε_1 molecules and exposed ε_2 molecules. Given that the ε_1 sublayer is only 8% of the QLL, however, most ε_2 molecules are exposed, and rather than introduce new terminology we employ these designations for both sublayers.

We proceed now to an examination of the layer-by-layer distribution of Euler angles, beginning with ε_1. Figure 9a represents the equilibrium distribution of Φ and $\cos(\Theta)$ for all molecules in this sublayer, obtained by averaging over 100 nanoseconds. The most probable orientation is dangling-O, with a dipole moment vector pointing slightly away from the surface ($\cos(\Theta)\approx 0.4$). A second pair of peaks corresponds to the dangling-H orientation. Figure 9b shows the distribution of angles for molecules adsorbing to ε_1. The

distribution is an average over 2-10 picoseconds after impact. Although not identical with the equilibrium distribution, the difference is not statistically significant. Time-resolved plots of the root-mean-square deviation from equilibrium (not shown here) imply that most of the orientational equilibration takes place within the first two picoseconds after striking the surface. Figure 9c represents the pre-sublimation picture of ε_1. It shows the distribution of Euler angles of a representative sample of sublimating molecules averaged over ten picoseconds just prior to sublimation. The predominant peak corresponds to a dangling-O orientation in which the dipole moment vector points closer to the surface normal ($\cos(\Theta)\approx 0.7$) than it does in the equilibrium distribution.

We next turn to an examination of the distribution of Euler angles of molecules in ε_2. Figure 9d represents the equilibrium picture of ε_2, based on 100 nanoseconds of simulation time. The distribution is similar to that of crystalline bulk bilayers, and distinctly different from ε_1. The broken left-right symmetry suggests that the formation of the QLL from the outermost bilayer occurs via depopulation of molecules from dangling-O and dangling-H (with $\cos(\Theta)<0$) orientations. Figure 9e represents the post-adsorption picture, 2-10 picoseconds after impact, for the molecules whose destination is the ε_2 sublayer. The predominant peaks correspond to orientations depleted in the equilibrium distribution for ε_2.

To obtain insight into the process of bulk accommodation, we examined the simulation results for layer-to-layer migrations. Figure 10 shows z-coordinates of oxygen atoms close to the surface, in which some permanent (>1 nanosecond) migrations have been

highlighted. We find that these migrations almost always occur as binary exchanges. For example, when the blue and green lines cross, an intra-bilayer exchange has occurred. When yellow and magenta cross, an interlayer exchange (or "interbilayer crossing"[36]) has occurred. The duration of an inter-bilayer exchange of the type $\varepsilon_1+\varepsilon_2 \leftrightarrow \mu_1$ is typically between 50 and 500 picoseconds.

Assuming first-order kinetics, we calculated e-folding lifetimes ($t_e = \sqrt{2}\, t_{1/2}$, where $t_{1/2}$ is the half-life) for inter- and intra-layer transitions, Table 2. These values were calculated according to

$$t_e = \frac{Number\ of\ molecules\ in\ source\ layer}{frequency\ of\ transitions} \tag{4}$$

where the numerator equals 128 for full bilayers, 118 for ε_2, and 10 for ε_1. Interlayer transitions were only counted if they persisted for more than ~1/2 nanosecond. We find that the lifetime of a molecule in ε_1 is shortest with respect to transitions to ε_2, about 200 picoseconds. Lifetimes pertaining to transitions $\varepsilon_1+\varepsilon_2 \leftrightarrow \mu_1$ and $\varepsilon_1+\varepsilon_2 \rightarrow$vapor are much longer, on the order of microseconds.

To obtain a value for the layer-specific bulk accommodation coefficient, it is necessary to choose a layer in the model to represent bulk ice. Layer μ_1 appears to be a good choice for this purpose. Molecules in μ_1 have the same mean and standard deviation vertical binding energy as molecules in deeper layers (Table 1). However, their H-bonds tend to

be of shorter duration (figure 3). Molecules in μ_1 are capable of moving out of their lattice positions, whereas deeper molecules are not (on an MD time scale). Taking μ_1 to be the beginning of bulk ice and assuming first-order kinetics, the bulk accommodation coefficient is obtained by[15]

$$\alpha_b = \alpha_s \frac{t_e^{-1}(QLL \rightarrow \mu_1)}{t_e^{-1}(QLL \rightarrow \mu_1) + t_e^{-1}(QLL \rightarrow vapor)} = 0.6 \qquad (5)$$

where t_e refers to layer lifetimes in Table 2. We emphasize that this result depends on the choice of μ_1 as the relevant bulk layer. If instead we chose a deeper bulk layer, we would infer a value approaching zero, since we observed no transitions to or from deeper layers during the course of our simulations.

IV. Discussion

Surface accommodation dynamics and the surface accommodation coefficient

Our value of α_s>0.99 is suggestively similar to results of previous work on QLL-free ice and on the surface of liquid water[16,20]. Is the mechanism the same for all cases? To investigate this question, we first show that a simple, "first encounter" mechanism is not supported by the present work, and then go on to consider the relevance of this observation. A "first-encounter" prediction can be constructed as follows:

1) A molecule approaching the surface will stick to the first molecule it encounters.

2) If the first molecule encountered is μ_1, the approaching molecule will adsorb as ε_2. If the first molecule encountered is ε_2 or ε_1, it will adsorb as ε_1.
3) The likelihood of first encounter with μ_1 is proportional to the number of vacant positions ("number vacancy") in ε_2.

Since 8% of QLL molecules are ε_1, it follows that the number vacancy of ε_2 is 8%, and the first-encounter prediction is a capture ratio of 92/8 ($\varepsilon_1/\varepsilon_2$). This result is significantly different from the 70/30 ($\varepsilon_1/\varepsilon_2$) ratio obtained here (figure 4). While recognizing that number vacancy does not translate directly into surface area vacancy, and that this model does not take into account ledge effects, the difference between 8% and 30% is large enough to suggest that adsorbing molecules respond in a more complex way to the surface than just sticking to the first molecule encountered.

In what way is the process more complex? It is useful to distinguish two possible views in this context, reorientation *vs* energy transfer. Regarding reorientation, Batista *et al*[20] found that high-energy molecules incident on an ordered, QLL-free, antiferroelectric ice surface favored two sites in particular, labeled "A" and "B". Site A accommodates dangling-O admolecules, and site B accommodates dangling-H admolecules. The reason incident water molecules stick to the surface, in this view, is that they reorient themselves on a timescale shorter than the time required for their lateral component of velocity to dissipate; without such reorientation, incident molecules would encounter strongly repulsive interactions and depart from the surface. The timescale for reorientation was reported to be on the order of a few tenths of a picosecond. Our results support the view

of fast orientational relaxation, inasmuch as figure 9b was prepared using data 2-10 picoseconds after hitting the surface, and indicates a distribution not significantly different from the equilibrium one.

From the viewpoint of energy transfer, Andersson *et al*[23] showed that water ice below 180 K captures gaseous argon molecules with near-100% efficiency, in a process characterized by effective transfer of energy to the ice surface. Those authors predicted that admolecules with mass close to argon would behave similarly. While the mass of a water molecule is less than half that of argon, it has much stronger intermolecular interactions with the ice surface. Our results support the rapid-energy-transfer view, inasmuch as thermal relaxation occurs quickly (~10 picoseconds), although as implied by the preceding discussion it takes place after orientational relaxation is complete.

Other authors have noted a separate distinction based on the *depth* of the accommodation site for foreign molecule adsorption. Mitlin *et al*[37], using MD-PMF for Xe adsorbed on the basal (0001) surface of ice, found two local minima they termed ε_1 and ε_2. Kroes and Clary[38] made similar observations for an HCl/ice system. Bishop *et al*[39] have speculated that "crevasses" in the QLL provide access to deeper layers in a way that leads to more effective trapping of adsorbed foreign species. Our results elaborate on this picture, showing that while the shallower destination (ε_1) is the more likely one, the deeper destination (ε_2) is responsible for more adsorption than one would expect on the basis of first-encounters. It may be of relevance to adsorption of foreign species, that water

molecules adsorbing to ε_2 do so initially in orientations that complement the existing, but depopulated, crystalline-like structure of that sublayer.

Sublimation dynamics and vapor pressure

Several ways of comparing the simulated result of $240 \pm 50\ Pa$ to experiment are possible. One is a direct comparison: At 250 K, the experimental[40,41] vapor pressure of ice is 76 *Pa*. Alternatively, one can compare melt-equivalent temperatures (nominal temperature minus melting temperature) at which the same vapor pressure prevails. The melting temperature of the NE6 model is 289 K[42]. Therefore, we find that a vapor pressure of 240 *Pa* corresponds to melt-equivalent temperatures of $-39°C$ and $-9°C$ for the simulation and real ice, respectively.

It is encouraging that the agreement is as close as it is, given that the NE6 potential was not optimized for this purpose. The estimated uncertainty in our result rules out the possibility that the simulated vapor pressure is higher than experiment merely because of poor statistics. Therefore, it is of interest to consider possible physical reasons for the discrepancy. A plausible possibility is that the high vapor pressure of the simulation is due to the lack of polarization in the NE6 potential, i.e., it is not possible to simultaneously represent bulk and vapor properties accurately without polarization[43]. A simple polarizable potential, practical for ice simulations (e.g., with a correct melting temperature) is, however, not available yet.

Bulk accommodation dynamics and the bulk accommodation coefficient

The millisecond-scale lifetimes we obtain for QLL$\leftrightarrow\mu_2$ transitions (table 2) are significantly longer than the lifetimes implied by Bolton and Pettersson's study of inter-bilayer hopping, despite their specification of a much lower model temperature of 210 K[36]. That study was based on the TIP4P model[44], however, which appears to have a much lower melting temperature of ~232 K[43], i.e., a melt-equivalent temperature of $-22°C$.

V. Conclusions

We have carried out a molecular dynamics study of near-equilibrium interactions between a QLL-covered ice slab with its vapor phase, at 250 K. Our purpose is to gain insight into the mechanics of sublimation and deposition, and on how structural properties of the QLL are relevant to those processes.

The outermost (ε_1) sublayer comprises 8% of the QLL. At equilibrium, molecules in this layer form two H-bonds, predominantly in a dangling-O orientation. A preference for a dangling-H orientation is also evident. The remaining 92% of QLL molecules belong to the deeper and thicker (ε_2) sublayer of the QLL. Molecules belonging to this sublayer are more crystalline, typically forming three H-bonds in an orientational distribution that closely resembles bulk crystalline ice. This distribution lacks the perfect symmetry of bulk crystalline ice, however, with the dangling-H and dangling-O orientations slightly depopulated; those molecules have pre-melted to form the ε_1 sublayer.

Regarding deposition, we find that >99% of water vapor molecules striking the surface are surface-accommodated (they "stick"), but that the detailed mechanism of sticking depends on the depth of their destination. 70% of sticking molecules are accommodated by the ε_1 sublayer. These admolecules achieve orientational relaxation within ~2 picoseconds. Thermal relaxation to an energy consistent with 2 H-bonds is complete within ~10 picoseconds.

The remaining 30% of adsorbing molecules are accommodated by the ε_2 sublayer. Orientational relaxation occurs within two picoseconds, primarily to depopulated orientations in ε_2. Initial thermal relaxation occurs within ~10 picoseconds, but not to the three H-bonds typical of ε_2 molecules, rather to the two H-bonds characteristic of ε_1 molecules. Finally, although this layer captures a higher percentage than what one would expect from first-encounter predictions (8%), this difference does not appear to be enthalpy-driven.

Regarding the mechanism of sublimation, molecules departing from the QLL do so primarily from the ε_1 sublayer, despite the fact that this sublayer constitutes only 8% of the QLL. Sublimation statistics are Poissonian. In the ten picoseconds prior to sublimation, departing molecules show a distinct preference for a dangling-O orientation that is slightly more outward-pointing (larger value of $\cos(\Theta)$) than the equilibrium distribution of ε_1 molecules.

Three parameters describing equilibrium ice-vapor interactions of the model system have been obtained. In addition to a surface accommodation coefficient of α_s>0.99, we find a layer-specific (μ_1) bulk accommodation coefficient of α_b=0.6. Sublimation occurs at a rate equivalent to P_{vap}=240±50 Pa.

Acknowledgements. This research was supported by the John Lantz Senior Sabbatical Fellowship and the Sabbatical Visit Program of the Institute of Organic Chemistry and Biochemistry of the Academy of Sciences of the Czech Republic (to S.N.). The work in Prague was performed within the framework of the research project Z40550506. Support from the Ministry of Education of the Czech Republic (grants LC512 and 1P05ME798) and from the US-NSF (grant CHE-0431312) is also gratefully acknowledged. We thank Dr. Milan Szöri for sharing his H-bond analysis code, Lubos Vrbka for providing ice slab initial conditions, and Victoria Buch for providing computer code that generates proton-disordered ice configurations, and for fruitful conversations.

References and notes

(1) Takano, Y.; Liou, K. N. *Journal of the Atmospheric Sciences* **1995**, *52*, 818-837.

(2) Kinne, S.; Liou, K. N. *Atmospheric Research* **1989**, *24*, 273-284.

(3) Neshyba, S. P; Grenfell, T. C.; Warren, S. G. *J. Geophys. Res.* **2003**, *108*, 4448.

(4) Grenfell, T. C.; Neshyba, S. P; Warren, S. G. *J. Geophys. Res.* **2005**, *110*, D17203.

(5) Gierens, K. M.; Monier, M.; Gayet, J. F. *J. Geophys. Res.* **2003**, *108*, 4069.

(6) Kärcher, B.; Lohmann, U. *J. Geophys. Res.* **2002**, *107*, 4698.

(7) Kärcher, B.; Lohmann, U. *J. Geophys. Res.* **2003**, *108*, 4402.

(8) Kärcher, B.; Lohmann, U. *J. Geophys. Res.* **2002**, *107*, 10.1029.

(9) Korolev, A. V.; Isaac, G. A.; Hallett, J. *Geophysical Research Letters* **1999**, *26*, 1299-1302.

(10) Monier, M.; Wobrock, W.; Gayet, J. F.; Flossmann, A. *Journal of the Atmospheric Sciences* **2006**, *63*, 504-525.

(11) Libbrecht, K. G. *J. Cryst. Growth* **2003**, *258*, 168–175.

(12) Vrbka, L.; Jungwirth, P. *Physical Review Letters* **2005**, *95*, 148501.

(13) Vrbka, L.; Jungwirth, P. *Journal of Molecular Liquids* **2007**, *134*, 64-70.

(14) Carignano, M. A.; Shepson, P. B.; Szleifer, I. *Molecular Physics* **2005**, *103*, 2957-2967.

(15) IUPAC Subcommittee for Gas Kinetic Data Evaluation, **2008**, http://www.iupac-kinetic.ch.cam.ac.uk.

(16) Vieceli, J.; Roeselová, M.; Tobias, D. J. *Chemical Physics Letters* **2004**, *393*, 249-255.

(17) Tsuruta, T.; Nagayama, G. *Journal of Physical Chemistry B* **2004**, *108*, 1736-1743.

(18) Morita, A.; Sugiyama, M.; Kameda, H.; Koda, S.; Hanson, D. R. *Journal of Physical Chemistry B* **2004**, *108*, 9111-9120.

(19) Winkler, P. M.; Vrtala, A.; Wagner, P. E.; Kulmala, M.; Lehtinen, K. E. J.; Vesala, T. *Physical Review Letters* **2004**, *93*, 075701.

(20) Batista, E. R.; Ayotte, P.; Bilic, A.; Kay, B. D.; Jonsson, H. *Physical Review Letters* **2005**, *95*, 223201-4.

(21) Suter, M. T.; Andersson, P. U.; Pettersson, J. B. C. *The Journal of Chemical Physics* **2006**, *125*, 174704.

(22) Nada. H.; van der Eerden, J. P. J. M. *The Journal of Chemical Physics* **2003**, *118*, 7401.

(23) Andersson, P. U.; Nagard, M. B.; Bolton, K.; Svanberg, M.; Pettersson, J. B. *Journal of Physical Chemistry B* **2000**, *104*, 2681-2688.

(24) Benjamin, I. *Physical Review Letters* **1994**, *73*, 2083-2086.

(25) Benjamin, I. *Accounts of Chemical Research* **1995**, *28*, 233-239.

(26) Benjamin, I. *J. Chem. Phys.* **1991**, *95*, 3698.

(27) Wilson, M. A.; Pohorille, A. *The Journal of Chemical Physics* **1991**, *95*, 6005-6013.

(28) Buch, V.; Sandler, P.; Sadlej, J. *Journal of Physical Chemistry B* **1998**, *102*, 8641-8653.

(29) Lindahl, E.; Hess, B.; van der Spoel, D. *Journal of Molecular Modeling* **2001**, *7*, 306-317.

(30) Yeh, I. C.; Berkowitz, M. L. *The Journal of Chemical Physics* **1999**, *111*, 3155.

(31) Suresh, S. J.; Naik, V. M. *The Journal of Chemical Physics* **2000**, *113*, 9727.

(32) Saito, Y. *Statistical Physics of Crystal Growth*; World Scientific: Singapore, 1996.

(33) Mathews, J.; Walker, R. L. *Mathematical Methods of Physics*; Addison Wesley: New York, 1970.

(34) Goldstein, H. *Classical Mechanics*; Addison-Wesley: Reading, 1980.

(35) Ikeda-Fukazawa, T.; Kawamura, K. *The Journal of Chemical Physics* **2004**, *120*, 1395.

(36) Bolton, K.; Pettersson, J. B. *Journal of Physical Chemistry B* **2000**, *104*, 1590-1595.

(37) S. Mitlin; A. S. Lemak; B. H. Torrie; K. T. Leung *Journal of Physical Chemistry B* **2003**, *107*, 9958-9963.

(38) Kroes, G. J.; Clary, D. C. *The Journal of Physical Chemistry* **1992**, *96*, 7079-7088.

(39) Bishop, C. L.; Pan, D.; Liu, L. M.; Tribello, G. A.; Michaelides, A.; Wang, E. G.; Slater, B. *Faraday Discuss.* **2009**,

(40) Buck, A. L. *Journal of Applied Meteorology* **1981**, *20*, 1527-1532.

(41) Marti, J.; Mauersberger, K. *Geophys. Res. Lett.* **1993**, *20*, 363-366.

(42) Abascal, J. L. F.; Garcia Fernandez, R.; Vega, C.; Carignano, M. A. *The Journal of Chemical Physics* **2006**, *125*, 166101-2.

(43) Vega, C.; Sanz, E.; Abascal, J. L. F. *The Journal of Chemical Physics* **2005**, *122*, 114507.

(44) Jorgensen, W. L.; Chandrasekhar, J.; Madura, J. D.; Impey, R. W.; Klein, M. L. *The Journal of Chemical Physics* **1983**, *79*, 926-935.

(45) Humphrey, W.; Dalke, A.; Schulten, K. *Journal of Molecular Graphics* **1996**, *14*, 33-38.

Tables

Table 1. Layer-specific vertical binding energies (BE)

layer	BE (kJ/mol)
ε_1	43±12[a]
ε_2	71±13
μ_1	88±6
$<\mu_{2\text{-}4}>$[b]	88±6

[a]one standard deviation
[b]mean values for layers μ_2-μ_4

Table 2. E-folding lifetimes with respect to layer transitions.

transition	t_e(ns)
$\varepsilon_1+\varepsilon_2 \rightarrow$ vapor	1200[a]
$\varepsilon_1+\varepsilon_2 \leftrightarrow \mu_1$	700[b]
$\varepsilon_1 \rightarrow \varepsilon_2$	0.2
$\varepsilon_2 \rightarrow \varepsilon_1$	3

[a]Based on 128 molecules in layer and a sublimation rate of 37 in 173 ns simulation time;
[b]only counting transitions lasting more than 0.5 ns

Figure Captions

Figure 1. Prismatic side-view of three unit cells, a few picoseconds after a sublimation event. Quasi-liquid layer formation is visible on basal (0001) surfaces at the top and bottom of the figure.

Figure 2. Density profile along the surface normal of oxygen atoms in a 10-nanosecond simulation. The inner layers (μ_i) exhibit bilayer doublets. The area under each doublet corresponds to 128 molecules. Sublayers ε_2 show somewhat degraded doublet structure, with areas implying ~118 molecules. Immediately adjacent to the vapor phase are the outermost sublayers, ε_1, with areas implying ~10 molecules. Stippling indicates the QLL.

Figure 3. Layer-by-layer distribution of long-lived (>1 nanosecond) H-bond coordination numbers.

Figure 4. Trajectories of rotationally and translationally equilibrated gas-phase molecules, at 250 K, initially located 1.5 nm from the basal surface. The one non-sticking trajectory in this set is highlighted.

Figure 5. Mean vertical binding energies of admolecules after striking the surface. Means were calculated after synchronizing trajectory times to the moment of impact, defined as time=0.

Figure 6. Z-coordinate trajectories of the oxygen atoms of twelve sublimating molecules prior to sublimation. Trajectory times have been synchronized such that the last moment bound is time=0.

Figure 7. Number of departures (sublimation events) in a 173-nanosecond simulation as a function of the time interval between departures, in 2-picosecond bins. Poisson distributions are obtained using Eq. 3.

Figure 8. VMD[45] depictions of molecular rotations by 3-1-3 Euler angles, plan view. Highlighted orientations on the right-hand-side of panel (a) are referred to in the text as "dangling-O". Highlighted orientations in the center of panel (b), with $\Theta \sim \pi/2$, are referred to as "dangling-H". Panel (c) highlights five ε_1 molecules.

Figure 9. Contour maps showing the layer-specific distribution of Euler angles for molecules in ε_1 and ε_2. More probable configurations are colored red. Panel (a), all ε_1 molecules in a 100-nanosecond simulation. Panel (b), 328 adsorbing molecules whose destination is ε_1, 2-10 ps after impact. Panel (c), sublimating molecules, 10-0 picoseconds before departure. Panel (d), all ε_2 molecules in a 100-nanosecond simulation. Panel (e), 124 adsorbing molecules whose destination is ε_2, 2-10 ps after impact.

Figure 10. Z-coordinate trajectories of oxygen atoms highlighting movement of water molecules between bilayers (turquoise, yellow, magenta) and within a bilayer (other colors). Time between markers is 50 picoseconds.

Figure 1.

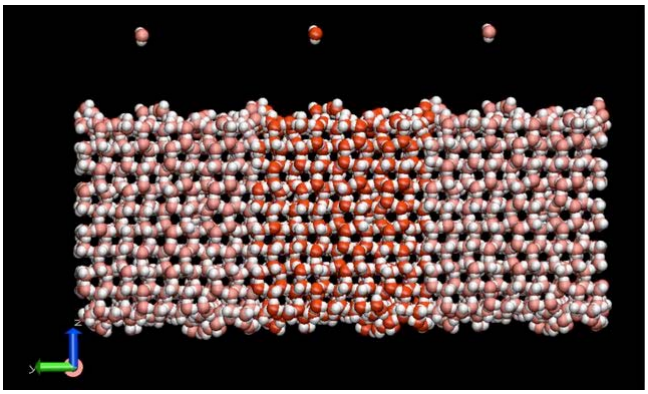

Figure 2.

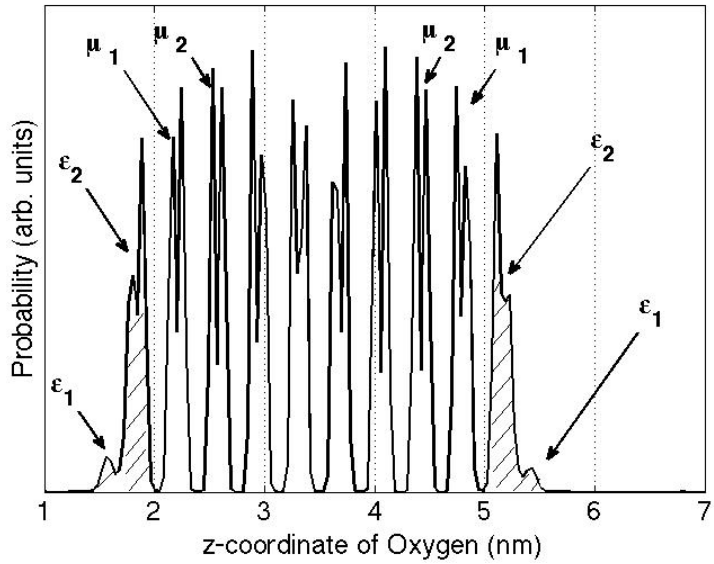
μ 1
μ 2
μ 2
μ 1
ε2
ε2
ε1
ε1
Probability (arb. units)
1
2
3
4
5
6
7
z-coordinate of Oxygen (nm)

Figure 3.

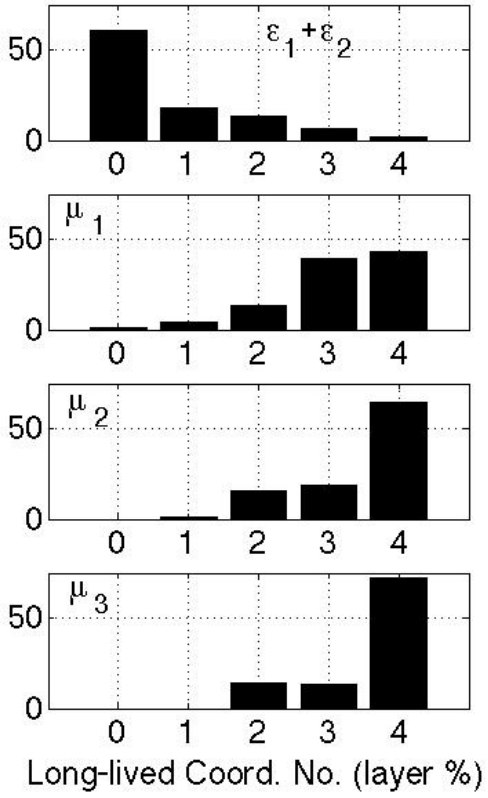

Figure 4.

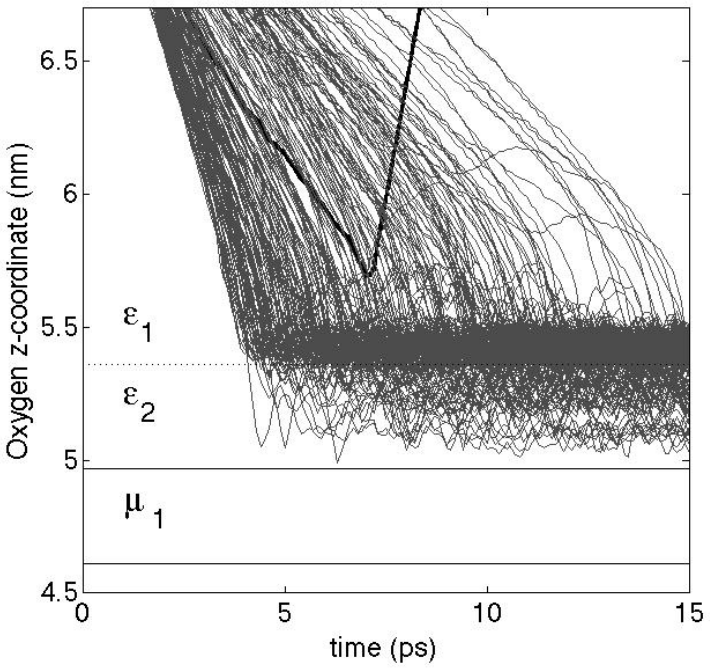

Figure 5.

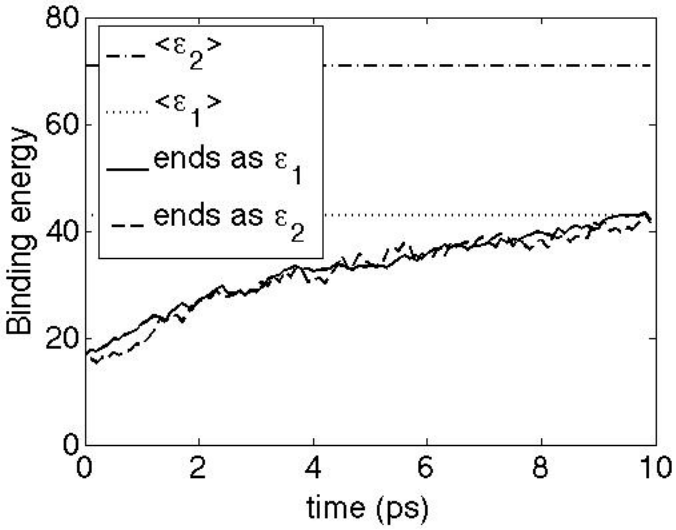
80
60
40
20
0
0
2
4
6
8
10
Binding energy
time (ps)
<ε2>
<ε1>
ends as ε1
ends as ε2

Figure 6.

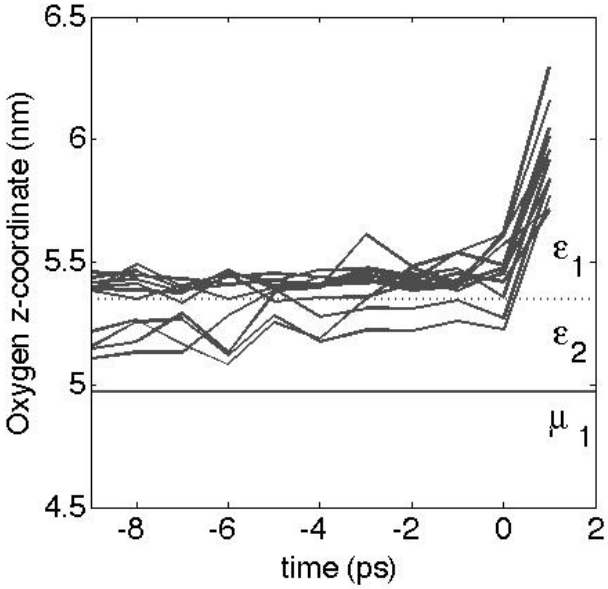

Figure 7.

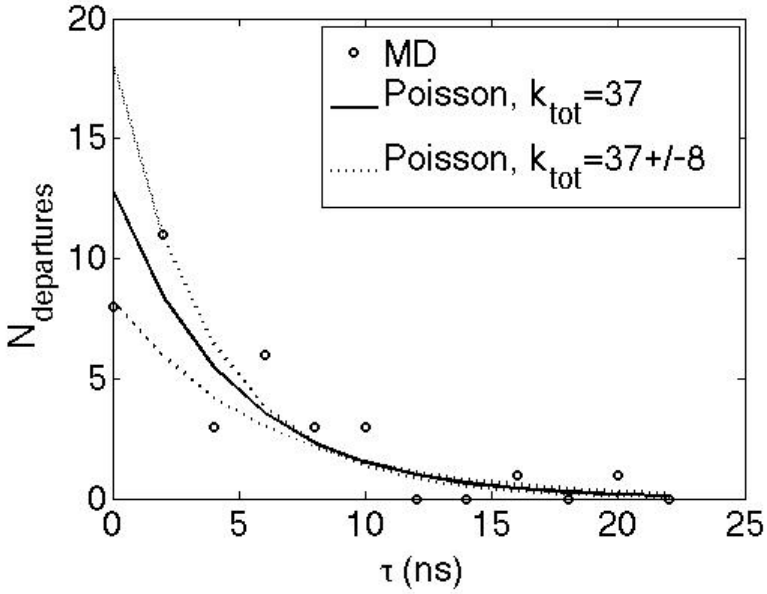
MD
Poisson, k_tot=37
Poisson, k_tot=37+/-8
N_departures
τ (ns)
0
5
10
15
20
25

Figure 8.

(a)

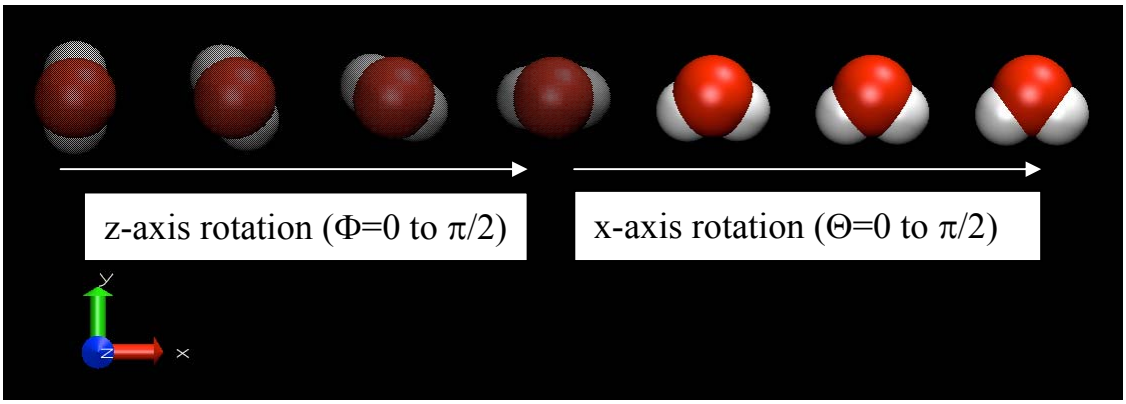
z-axis rotation (Φ=0 to π/2)
x-axis rotation (Θ=0 to π/2)

(b)

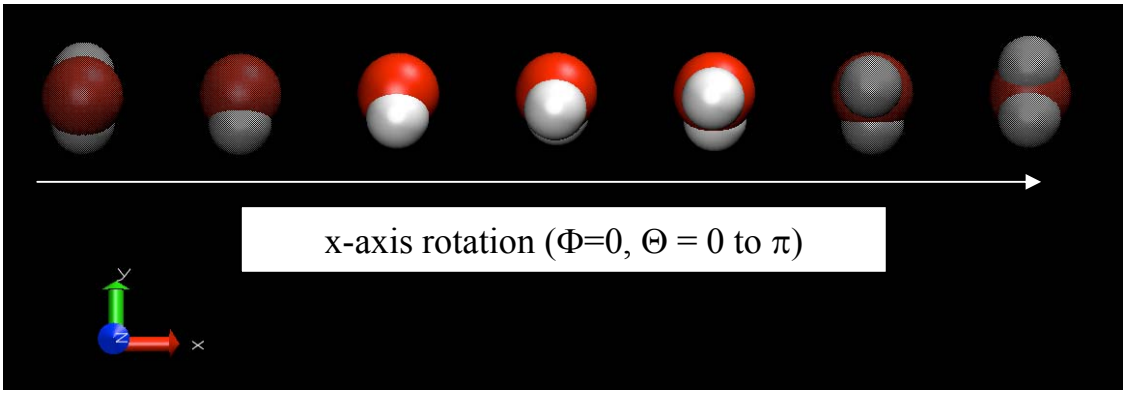
x-axis rotation (Φ=0, Θ = 0 to π)

(c)

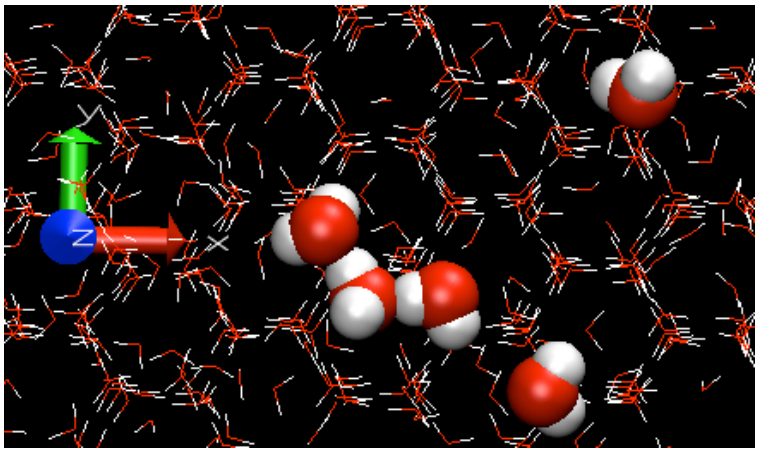

Figure 9.

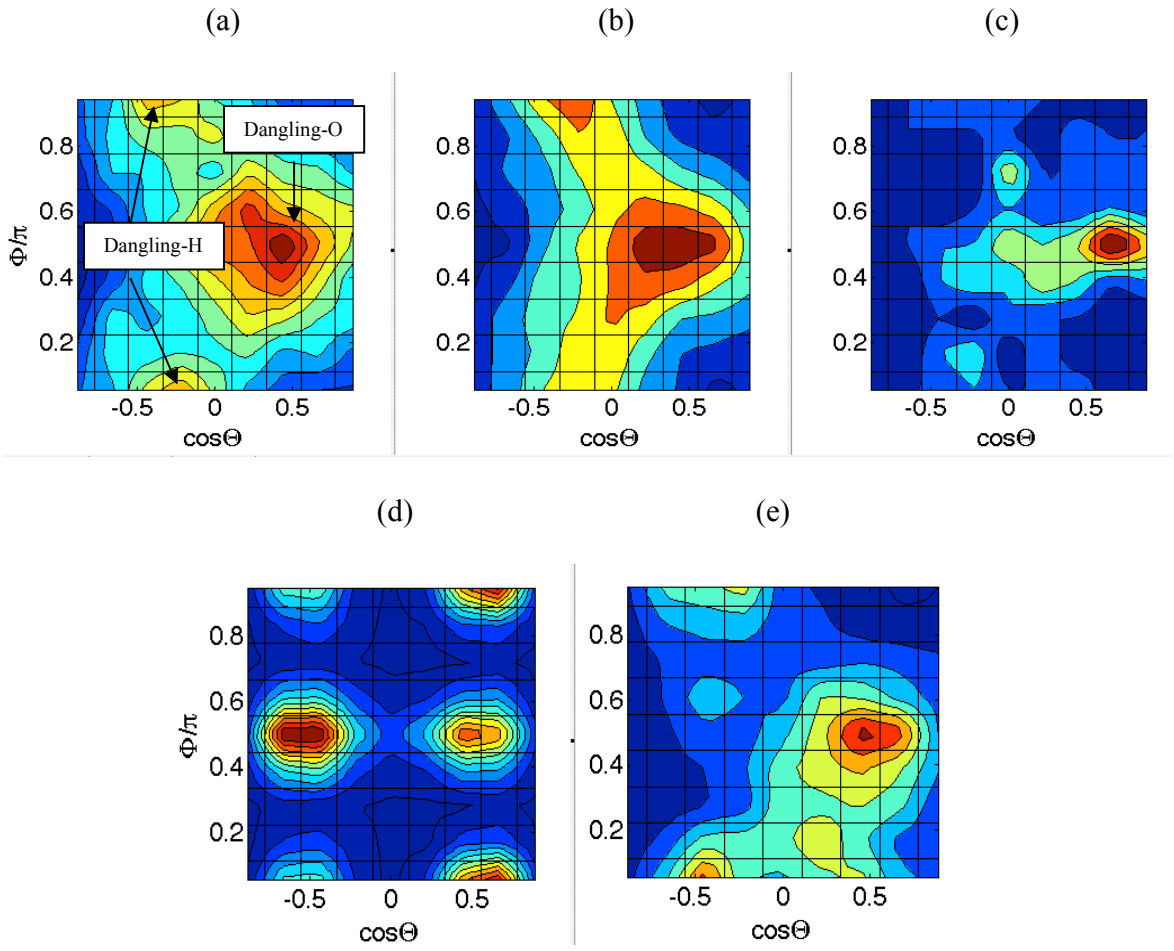

Figure 10.